



FULL PAPER

Application of new Ru (II) pyridine-based complexes in the partial oxidation of *n*-octane

Revana Chanerika | Holger B. Friedrich | Mzamo L. Shoji

School of Chemistry and Physics,
University of KwaZulu-Natal, Durban,
South Africa

Correspondence

Holger B. Friedrich, School of Chemistry
and Physics, University of KwaZulu-Natal,
Durban, South Africa.
Email: friedric@ukzn.ac.za

Funding information

c*change, Grant/Award Number: PAR06;
National Research Foundation, Grant/
Award Number: 111508

Abstract

Tridentate and bidentate Ru (II) complexes were prepared through reaction of four pyridine-based ligands: pyCH₂N(R)CH₂py {R = propyl, *tert*-butyl, cyclohexyl and phenyl; py = pyridine} with the [(η⁶-C₆H₆)Ru(μ-Cl)Cl]₂ dimer. Crystal structures of the new tridentate Ru (II) complexes [Ru{pyCH₂N(R)CH₂py}C₆H₆](PF₆)₂ (R = C₃H₇ (**1**), C(CH₃)₃ (**2**), C₆H₁₁ (**3**)) and the bidentate Ru (II) complex [Ru{pyCH₂N(R)}C₆H₆]PF₆ (R = C₆H₅ (**4**)) are reported. It was found that complexes **1**, **2**, **3** and **4** crystallised as mono-metallic species, with a piano stool geometry around each Ru centre. All complexes were active in the selective oxidation of *n*-octane using *t*-BuOOH and H₂O₂ as oxidants. Complexes **2** and **4** reached a product yield of 12% with *t*-BuOOH as oxidant, however, superior yields (23–32%) were achieved using H₂O₂ over all systems. The selectivity was predominantly towards alcohols (particularly 2-octanol) over all complexes using *t*-BuOOH and H₂O₂ after reduction of the formed alkylhydroperoxides in solution by PPh₃. High TONs of up to 2400 were achieved over the Ru/H₂O₂ systems.

KEYWORDS

alcohols, bidentate, NNN ligands, oxidation, ruthenium complexes

1 | INTRODUCTION

C-H bond activation or functionalization has been a matter of interest over several years in an attempt to establish new grounds from a synthetic perspective and also provide alternative and green methods for the preparation of organic compounds.^[1] In this regard, the design and development of efficient catalyst systems to activate C-H bonds is of great importance. Therefore, it is crucial to understand the stoichiometric or catalytic principles that influence such transformations. To study such process requires a careful design of ligands and catalysts suitable for the activation of C-H bonds.^[1]

Carbon-hydrogen bonds are deemed inert since they are far less reactive than carbon-oxygen or carbon-halogen moieties.^[2,3] In this sense, the inert C-H bond should

be activated to a C-X functionality, with X being either, I, Br, Cl, OTf, OTs, etc. Alkanes are among the least reactive class of organic hydrocarbons as they constitute of strong C sp³-H bonds and single C sp³-C sp³ bonds.^[4] Transition metals provide a possible route to functionalising inert C-H bonds.^[5]

Over the past four decades, much attention has been drawn to developing homogeneous catalysts for their advantages over heterogeneous systems, such as milder reaction conditions, higher selectivity, and an enhanced range of transformation modes.^[4] Many desirable properties arise from the coordination of a multidentate ligand to a specific metal, such as the reduction of leaching (dissociation of the ligand from the metal). The lability of the complex may be fine-tuned by the donor atoms and substituents present on the complex, thereby influencing the

metal electron density as well as the coordination of substrates to the metal.^[6] This controls the electronic and steric properties of the metal as a whole.

Ligands containing nitrogen donors have gained attention in various fields, including homogeneous catalysis, coordination chemistry and organic synthesis. Research conducted in recent years has revealed applications of planar tridentate NNN ligands in materials, physical chemistry, homogenous catalysis and organic synthesis.^[7–9] In contrast, reports on unsymmetrical planar tridentate NNN ligands bound to various transition metals have only been sporadic.^[10]

Recent developments in ruthenium pincer complexes have shown new reactivities in activating strong chemical bonds and several serve as efficient catalysts for various reactions, including green transformations.^[11] Zeng and Yu have reported efficient hemilabile Ru (II) NNN complexes incorporating an unsymmetrical 2-(benzoimidazol-2-yl)-6-(pyrazole-1-yl) pyridine ligand in the transfer hydrogenation of ketones.^[12] A report by Sarkar *et al.* describes bidentate and tridentate Ru (II) carbonyl complexes bearing thioarylazimidazole ligands, with the bidentate catalyst exhibiting the highest activity in the oxidation of alcohols by N-methylmorpholine-N-oxide.^[13] Recently we reported new (η^5 -cyclopentadienyl)dicarbonylruthenium (II) amine complexes in the oxidation of styrene, with a dinuclear complex, $[(\eta^5\text{-C}_5\text{H}_5)\text{Ru}(\text{CO})_2\text{NH}_2(\text{CH}_2)_3]_2[\text{BF}_4]_2$, demonstrating the best activity with yields reaching 95%.^[14] In a further study, Ru (II) *N,N'*-bidentate complexes incorporating pyridyl-imine ligands for the transfer hydrogenation of cyclohexanone were reported with high yields and TONs of 1990.^[15]

To the best of our knowledge, there are few to no reports on NNN-pyridine based Ru (II) complexes in the activation of paraffinic C-H bonds, however, the use of a few related compounds in several other applications has been reported.^[16–22] As part of our continuing work on

complexes with N-donor ligands, where we have previously reported analogous Co (II) tridentate complexes.^[23]

The present work investigated the catalytic activity of four new pyridine-based ruthenium systems in the partial oxidation of *n*-octane. It further investigated the stability, steric effects, and electronic effects of the complexes by varying the N-donor backbone from propyl, *tert*-butyl, cyclohexyl and phenyl groups as depicted in Figure 1.

2 | EXPERIMENTAL

2.1 | General

All experimental manipulations of the ruthenium compounds were carried out under inert gas using standard Schlenk techniques unless otherwise noted. All reaction glassware was oven dried. Solvents were dried prior to use according to established methods.^[13] Chemicals utilized in ligand synthesis, including 2-pyridine methanol (98%), propylamine (98%), *tert*-butylamine (98%), cyclohexylamine (99%), aniline (99%) and tetrabutylammonium bromide (TBAB), were purchased from Sigma-Aldrich and used as received. Ruthenium (III) chloride hydrate was sourced from DLD Scientific. The two oxidants, *t*-BuOOH and H₂O₂, were purchased from Sigma Aldrich and DLD Scientific, respectively. The ¹H and ¹³C NMR spectra of all ligands and diamagnetic ruthenium compounds were recorded using a Bruker Avance 400 MHz spectrophotometer and are reported as chemical shifts (δ , ppm) with reference to the solvent peak, dimethylsulfoxide-*d*₆ (m, 2.50 ppm). Chemical shifts (δ , ppm) of peaks in the proton decoupled ¹³C NMR data are referenced to the DMSO-*d*₆ solvent peak (39.51 ppm) with the specific carbon indicated in parentheses. IR spectra were recorded using a Perkin Elmer Attenuated Total Reflectance (ATR) spectrophotometer between 4000–380 cm⁻¹. Elemental analyses were

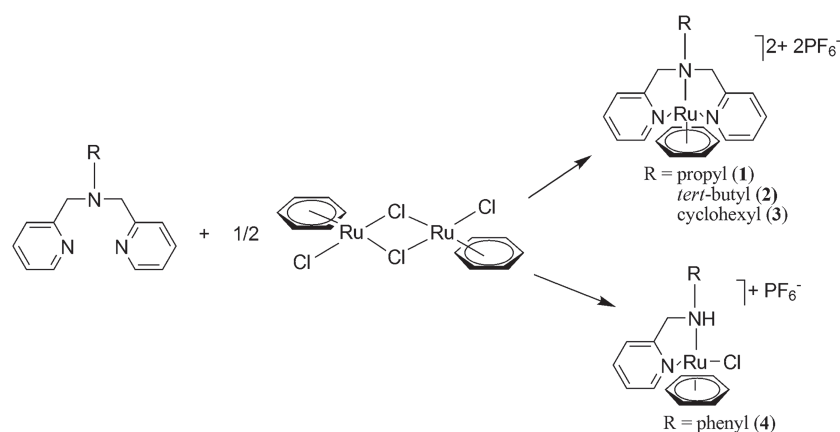


FIGURE 1 Synthesis of Ru[pyCH₂N(R)CH₂py]C₆H₆(PF₆)₂ (1–3) and Ru[pyCH₂NH(R)]ClC₆H₆PF₆ (4)

recorded on a ThermoScientific Flash 2000 CHNS/O analyzer. High and low resolution mass spectrometric data were obtained on a Bruker Micro TOF-Q11 using an electron spray ionisation (ESI) technique, with a sample concentration of 10 ppm. The ligands **L1** [pyCH₂NC₃H₇CH₂py], **L2** [pyCH₂NC(CH₃)₃CH₂py], **L3** [pyCH₂NC₆H₁₁CH₂py], **L4** [pyCH₂NC₆H₅CH₂py] and precursor, 2-chloromethylpyridine hydrochloride, were prepared as described previously.^[23]

2.2 | Synthesis of the [(η⁶-C₆H₆)Ru(μ-Cl)Cl]₂ dimer

The [(η⁶-C₆H₆)Ru(μ-Cl)Cl]₂ dimer was synthesised in a similar manner to the report by Bennet and Smith.^[24] To a 100 ml nitrogen saturated round bottom flask, 0.5 g RuCl₃·xH₂O was added in 25 ml ethanol. The mixture was allowed to stir, after which 2.5 ml of 1,4-cyclohexadiene was added. The brown precipitate, which formed after a 4 hr reflux, was collected under vacuum filtration and washed with a small portion of methanol. The resultant solid was dried *in vacuo*.

2.3 | Synthesis of [Ru{pyCH₂NC₃H₇CH₂py}C₆H₆](PF₆)₂ (1)

To a 100 ml round bottom flask containing a mixture of **L1** (0.29 g, 1.20 mmol) in 40 ml of methanol, [(η⁶-C₆H₆)Ru(μ-Cl)Cl]₂ (0.3 g, 0.6 mmol) was added. The mixture was allowed to stir at room temperature for 24 hr during which the color of the solution changed to a dark-brown color. The solution was concentrated to ~7 mL after which NH₄PF₆ (0.20 g, 1.20 mmol) was added and stirred for 1 hr. The resulting precipitate was filtered off and washed with a small portion of cold methanol and diethyl ether. The crude product was purified by dissolving the solid in acetonitrile, filtering off the undissolved material and precipitating the product with diethyl ether. The resulting dark-green crystalline solid was dried *in vacuo* for several hours and recrystallized by vapor diffusion of diethyl ether into a concentrated acetonitrile solution, yielding crystals suitable for X-ray diffraction (0.32 g, 75%). ¹H NMR (DMSO): δ 1.0 (t, 3H, *J* = 7.1 Hz, CH₃-prop), 1.8 (m, 2H, CH₂-prop), 4.0 (m, 2H, prop-CH₂-N), 4.4; 4.8 (d, 2H, *J* = 16.9 Hz; d, 2H, *J* = 17.4 Hz, N-CH₂-py), 6.3 (s, 6H, C₆H₆), 7.5 (m, 2H, CH-py), 7.4 (d, 2H, *J* = 7.5 Hz, CH-py), 7.9 (ddd, 2H, *J* = 8.8, 7.7, 1.0 Hz, CH-py), 9.2 (d, 2H, *J* = 5.6 Hz, CH-py). ¹³C NMR (DMSO): δ 10.9 (CH₃-prop), 17.8 (CH₂-prop), 68.4 (CH₂-N-py), 70.1 (prop-CH₂-N), 88.3 (C₆H₆), 122.4 (CH-py), 125.6 (CH-py), 140.3 (CH-py), 154.4 (CH-

py), 160.5 (C-py). IR ν_{max} (cm⁻¹): 1609 (s) (C-C aromatic), 1440 (s) (C-H alkyl), 779 (s) (C-H rocking). m/z (calcd): 210 (210.56). Melting point: 220.7–224.8 °C. Elemental analysis for C₂₁H₂₅N₃RuP₂F₁₂: calcd C, 35.5; H, 3.6; N, 5.9; found C, 35.6; H, 3.6; N, 6.1.

2.4 | Synthesis of [Ru{pyCH₂NC(CH₃)₃CH₂py}C₆H₆](PF₆)₂ (2)

Complex **2** was prepared analogously to **1** using **L2** (0.20 g, 0.78 mmol); [(η⁶-C₆H₆)Ru(μ-Cl)Cl]₂ (0.20 g, 0.39 mmol) and NH₄PF₆ (0.13 g, 0.78 mmol) was added to the yellow colored solution. The obtained mustard powder was dried *in vacuo* for several hours and recrystallized upon vapor diffusion of diethyl ether into a concentrated acetonitrile solution, yielding crystals suitable for X-ray diffraction (0.27 g, 94%). ¹H NMR (DMSO): δ 1.6 (s, 9H, CH₃-*t*but), 3.9; 4.9 (d, 2H, *J* = 17.3 Hz; d, 2H, *J* = 17.2 Hz, N-CH₂-py), 6.4 (s, 6H, C₆H₆), 7.6 (ddd, 2H, *J* = 7.7, 6.5, 0.9 Hz, CH-py), 7.5 (d, 2H, *J* = 7.8 Hz, CH-py), 8.0 (ddd, 2H, *J* = 8.8, 7.7, 1.0 Hz, CH-py), 9.3 (d, 2H, *J* = 6.2 Hz, CH-py). ¹³C NMR (DMSO): δ 63.4 (CH₃-*t*but), 68.7 (N-CH₂-py), 88.5 (C₆H₆), 121.4 (CH-py), 122.6 (CH-py), 135.8 (CH-py), 148.1 (CH-py), 161.9 (C-py). IR ν_{max} (cm⁻¹): 1613 (w) (C-C aromatic), 1448 (w) (C-H alkyl), 779 (s) (C-H rocking). m/z (calcd): 217.56 (217.06). Melting point: 287.1–288.7 °C. Elemental analysis for C₂₂H₂₇N₃RuP₂F₁₂: calcd C, 36.5; H, 3.8; N, 5.8; found C, 36.0; H, 3.6; N, 5.2.

2.5 | Synthesis of [Ru{pyCH₂NC₆H₁₁CH₂py}C₆H₆](PF₆)₂ (3)

Complex **3** was prepared analogously to **1** using **L3** (0.20 g, 0.71 mmol); [(η⁶-C₆H₆)Ru(μ-Cl)Cl]₂ (0.18 g, 0.36 mmol) and NH₄PF₆ (0.17 g, 0.71 mmol) was added to the yellow colored solution. The obtained yellow powder was dried *in vacuo* for several hours and recrystallized upon vapor diffusion of diethyl ether into a concentrated acetonitrile solution, yielding crystals suitable for X-ray diffraction (0.21 g, 79%). ¹H NMR (DMSO): δ 1.2 (m, 2H, CH₂-cy), 1.6 (q, 2H, *J* = 9.1 Hz, CH₂-cy), 1.7 (m, 2H, CH₂-cy), 1.8 (m, 2H, CH₂-cy), 2.2 (m, 2H, CH₂-cy), 4.1 (m, 2H, CH₂-cy), 4.0; 4.8 (d, 2H, *J* = 17.3 Hz; d, 2H, *J* = 15.6 Hz, N-CH₂-py), 6.3 (s, 6H, C₆H₆), 7.6 (ddd, 2H, *J* = 7.8, 6.8, 1.0 Hz, CH-py), 7.6 (d, 2H, *J* = 7.8 Hz, CH-py), 8.1 (ddd, 2H, *J* = 8.6, 8.0, 1.5 Hz, CH-py), 9.3 (d, 2H, *J* = 5.6 Hz, CH-py). ¹³C NMR (DMSO): δ 24.2 (CH₂-cy), 25.2 (CH₂-cy), 25.4 (CH₂-cy), 28.0 (CH₂-cy), 32.9 (CH₂-cy), 74.0 (N-CH₂-py), 59.3 (CH-cy), 89.5 (C₆H₆), 123.0 (CH-py), 126.3 (CH-py), 141.0 (CH-py), 155.6 (CH-

py), 162.3 (C-py). IR ν_{\max} (cm⁻¹): 1611 (w) (C-C aromatic), 1461 (w) (C-H alkyl), 771 (s) (C-H rocking). m/z (calcd): 230.57 (230.06). Melting point: 237–241.3 °C. Elemental analysis for C₂₄H₂₉N₃RuP₂F₁₂: calcd C, 38.4; H, 3.9; N, 5.6; found C, 38.8; H, 4.0; N, 5.5.

2.6 | Synthesis of [Ru{pyCH₂NHC₆H₅}C₆H₆]PF₆ (4)

Complex **4** was prepared analogously to **1** using **L4** (0.20 g, 0.73 mmol); [(η⁶-C₆H₆)Ru(μ-Cl)Cl]₂ (0.18 g, 0.36 mmol) and NH₄PF₆ (0.12 g, 0.73 mmol) was added to the brown colored solution. The dark-brown crystalline solid was dried *in vacuo* for several hours and recrystallized upon vapor diffusion of diethyl ether into a concentrated acetonitrile/methanol solution, yielding crystals suitable for X-ray diffraction (0.26 g, 95%). ¹H NMR (DMSO): δ 4.4; 5.2 (d, 1H, *J* = 14.9 Hz; m, 1H, N-CH₂-py), 5.4 (s, 6H, C₆H₆), 7.4 (m, 1H, CH-ph), 7.5 (d, 1H, *J* = 7.8 Hz, CH-py), 7.6 (m, 1H, CH-py), 7.6 (m, 4H, CH-ph), 8.1 (ddd, 1H, *J* = 8.7, 7.6, 1.5 Hz, CH-py), 9.2 (d, 1H, *J* = 5.9 Hz, CH-py). ¹³C NMR (DMSO): δ 58.9 (N-CH₂-py), 87.2 (C₆H₆), 119.3 (CH-ph), 125.2 (CH-py), 126.0 (CH-py), 129.4 (CH-ph), 139.6 (CH-py), 155.1 (CH-py), 159.5 (C-py). IR ν_{\max} (cm⁻¹): 1597 (w) (C-C aromatic), 1427 (w) (C-H alkyl), 763 (s) (C-H rocking). m/z (calcd): 399.02 (399.02). Melting point: 237.6–241.4 °C. Elemental analysis for C₁₈H₁₈N₂RuClPF₆: calcd C, 39.7; H, 3.3; N, 5.2; found C, 40.0; H, 3.3; N, 5.6.

2.7 | X-ray analyses

Selected crystals of complexes **1–4** were glued onto the tips of glass fibers and mounted in a stream of cold nitrogen (173 K). Each crystal was centered in the X-ray beam with the aid of a video camera. Single crystal X-ray diffraction data and evaluation was performed on a Bruker Smart APEXII diffractometer with graphite monochromated Mo K_α radiation (50 kV, 30 mA and λ = 0.71073 Å) using the APEXII^[25] data collection software. Data collection was carried out at 100(2) K and the temperature was controlled by an Oxford Cryostream cooling system (Oxford Cryostat) operating at 100(1) K. The collection method involved ω-scans of width 0.5° and 512 x 512 bit data frames. Data reduction and cell refinement were performed using the program SAINT.^[26] The data were scaled and absorption corrections performed using the SADABS^[27] multi-scan technique. The structures were solved by direct methods using SHELXS.^[28] Isotropic refinement was first done on non-

hydrogen atoms, followed by anisotropic refinement by full-matrix least-squares methods based on F² using SHELXL.^[28] Structural diagrams and publication material were generated using SHELXL,^[28] PLATON,^[29] X-Seed,^[30,31] POV-Ray^[32] and MERCURY.^[33] Reports were subjected to online check cif validation showing no structural disorder in **1–4**. Supplementary crystallographic data for compounds **1–4** can be obtained from CCDC 1940854–1940857 via www.ccdc.cam.ac.uk/data_request/cif.

2.8 | Oxidation of *n*-octane

Paraffin oxidation studies were performed under inert conditions in moisture free glassware using dry solvents. The *n*-octane to compound ratio was kept constant at 1:100 unless otherwise stated. A mass of 10 mg of cyclopentanone as the internal standard was loaded each time into a 50 ml two-neck pear shaped flask. Each mixture comprised of ~6 mg of Ru complexes, **1–3**, or ~3 mg of the bidentate complex **4**, in 10 ml of acetonitrile, together with the hydrocarbon substrate (0.008 mmol) and internal standard (~10 mg). The oxidants (*t*-BuOOH or H₂O₂) were added at differing ratios relative to the amount of substrate added (1:3, 1:6, 1:9, 1:12, 1:15 for *t*-BuOOH and 1:6, 1:9, 1:12 for H₂O₂) from which the optimum ratio of 1:12 for the Ru/*t*-BuOOH (~32 mmol) and Ru/H₂O₂ (~42 mmol) complexes, respectively, were established. At pre-established optimum conditions, an aliquot of the mixture was removed with a Pasteur pipette and PPh₃ was added prior to filtering through silica. Of this mixture, 0.5 μL was injected into a Perkin Elmer Claurus 580 Auto System Gas chromatograph integrated with a Flame Ionisation Detector (FID) for quantification of the product stream. All data are a result of an average of two individual runs with differences reported to within 1%. Column specifications and GC parameters are listed in the supplementary information (Table S1). Studies investigating the mechanism of the catalytic system were done using the radical scavenger, 2,2,6,6-tetramethylpiperidine-1-oxyl (TEMPO) with five equivalent additions relative to the substrate.

3 | RESULTS AND DISCUSSION

The synthesis and characterization of four new Ru complexes are described in which **1–3** contain a di-pyridyl NNN ligand system, with R groups, propyl, *tert*-butyl and cyclohexyl, on the central N-donor atom that is bound to two constrained six membered pyridine rings *via* two individual methylene linkers. Complex **4** incorporates a

single pyridine ring linked to a phenyl substituted N-donor backbone *via* one methylene group.

The formation of the intended compounds was indicated through color changes observed during each reaction with the $[(\eta^6\text{-C}_6\text{H}_6)\text{Ru}(\mu\text{-Cl})\text{Cl}]_2$ precursor and respective ligand. The structures and geometries of these compounds were established through single crystal X-ray diffraction, together with elemental analysis, IR and NMR spectroscopies. Noted differences between the melting points of **1–4** versus their starting materials also showed successful complexation.

Ru (II) forms a diamagnetic low spin complex and as a result NMR studies could be easily carried out. The aromatic proton signals of **1–4** show significant shifts relative to those observed in the ^1H NMR spectra of the uncoordinated ligands, confirming coordination.^[34] Apart from these resonance shifts, distinct singlets around 5.5–6.4 ppm, due to the protons of the benzene ring in the Ru complexes, further confirms successful complexation. The singlet, centered around 3.7–4.3 ppm in the free ligands (assigned to the methylene protons), splits into two doublets on coordination, with the first at around 3.9–4.4 ppm and the other at 4.8–5.2 ppm, due to these becoming diastereotopic (Table 1).^[35–38] Moreover, the methylene linker separating the aliphatic/aromatic and pyridine fragments of the ligand is affected by the planarity of the substituent on the central N-donor atom. Therefore, the split CH_2 signals are also due to the pyridine rings and central nitrogen substituents appearing in two different planes to each other.^[39]

Compound **4** forms a bidentate complex which was confirmed by X-ray diffraction, as well as NMR, MS and elemental analysis. A few examples of similar chemistry are known,^[40,41] and cleavage of a side arm of a multi-dentate ligand is rare but not unknown.^[42]

Apart from a clear shift in the C-H alkyl stretch and bend, C-C aromatic and C-H rocking vibrational bands between the coordinated and uncoordinated ligands (supplementary information, Table S2), it is worth noting that the C=N vibration is generally strong, as opposed to the corresponding peak appearing in the uncoordinated ligand (Table 1).^[43] This observation is noticeable in all

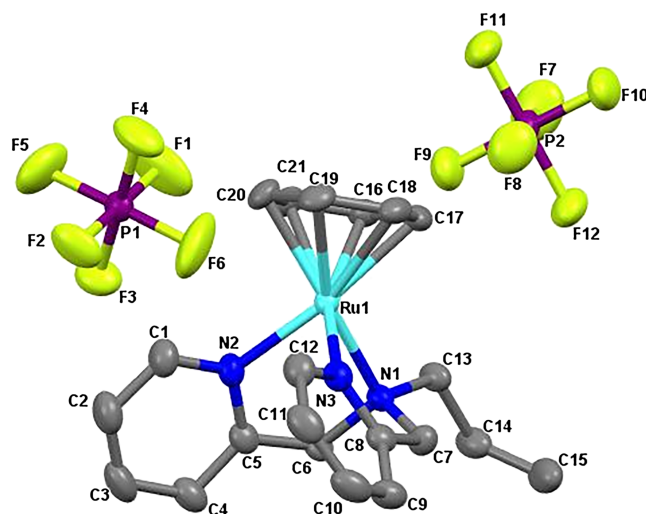


FIGURE 2 Single crystal structure of complex **1** drawn at 50% thermal ellipsoid probability, with omission of hydrogen atoms for clarity

complexes, which shows coordination of the pyridine rings to the Ru metal. Furthermore, an intense PF_6^- band is seen at 828 cm^{-1} .^[44] All other bands seen in the IR spectra of the Ru complexes were low in intensity. Also, synthesis of these complexes was further confirmed by mass spectrometry and single crystal XRD results, shown later.

3.1 | Crystal structures of 1–4

The Ru complexes with the different N-bonded R groups (**1–4**) all exhibit a piano-stool geometry^[45] (Figures 2–5), with **1–3** crystallizing in the monoclinic $P2_1/c$ space group and **4** in $P2_1/n$. All complexes exist as monomeric units due to the metal ion being stabilized through electron donation from the nitrogen atoms and aliphatic moieties on the central N-donor backbone, thus preventing dimerization.

The Ru atom in **1–3** binds to the three N-donor atoms in a terdentate fashion, and to the electron rich benzene ring. The NNN coordinating ligand occupies the positions as the legs of the piano stool, whilst the benzene ring,

TABLE 1 ^1H NMR and IR shifts of the complexes relative to those observed in the ligands

Complex	^1H NMR IR $\nu_{\text{max}}/\text{cm}^{-1}$			
	Ligand (CH_2)	Complex (CH_2)	Ligand(C=N)	Complex (C=N)
1	3.7	4.4, 4.8	1667	1609
2	3.8	3.9, 4.9	1589	1613
3	3.8	4.0, 4.8	1588	1611
4	4.3	4.4, 5.2	1597	1602

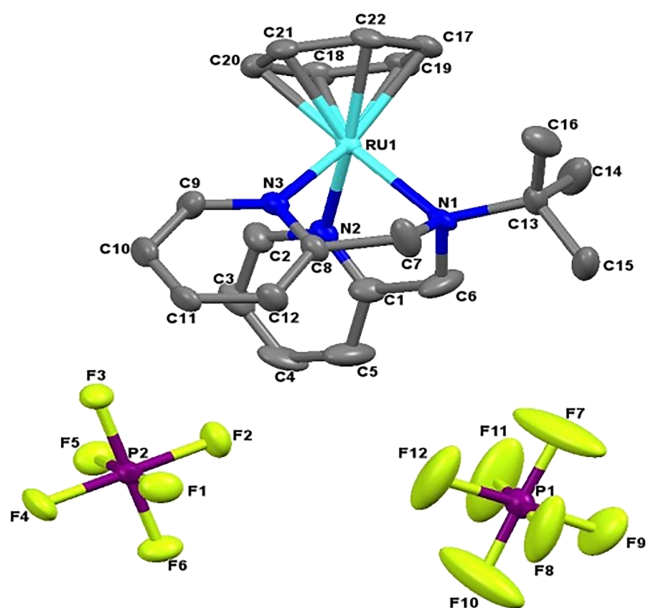


FIGURE 3 Single crystal structure of complex **2** drawn at 50% thermal ellipsoid probability, with omission of hydrogen atoms for clarity

occupying the remaining coordination sites, takes up the position as the seat of the piano stool. The Ru center in **4** is coordinated to the nitrogen atoms of the pyridine and the phenyl ring, and a chlorine atom as the base of the stool, with the benzene occupying the apex of the stool.

Selected bond lengths and angles of crystal structures **1–3** are given in Table 2. Crystallographic and structure refinement data for all complexes are presented in the supporting information (Table S3). The Ru-Cg distance (the distance of the Ru to the midpoint of the benzene ring) of 1.462 Å for **1** is comparable to the Ru-Cg distance of 1.463 Å for **3**. However, in complex **2**, the Ru-Cg

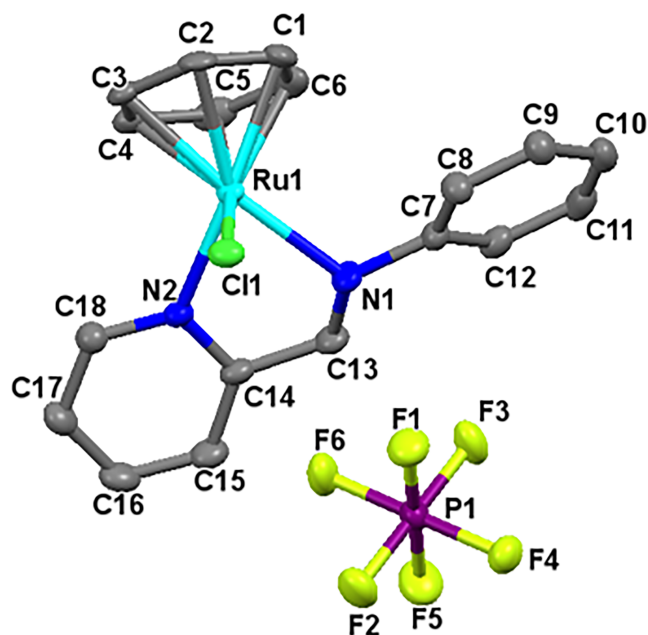


FIGURE 5 Single crystal structure of complex **4** drawn at 50% thermal ellipsoid probability, with omission of hydrogen atoms for clarity

distance is 1.470 Å, showing that the benzene ring in this case is bound more weakly to the metal ion with a more limited flow of electrons from the benzene ring to the metal.^[20]

In **3**, the N(1)-Ru(1) distance of 2.177(4) Å is shorter in comparison to the distance (2.242(3) Å) in complex **2**, suggesting that the Ru may be more electron rich. The N(2)-Ru(1)-N(1) bite angle is more acute for **3** (76.22(18)°) than for **2** (79.23(18)°) and **1** (80.63(10)°), which tend more closely to the tridentate facial coordination angle of 90°. This implies greater steric hindrance around the metal center in **3**, with a less open

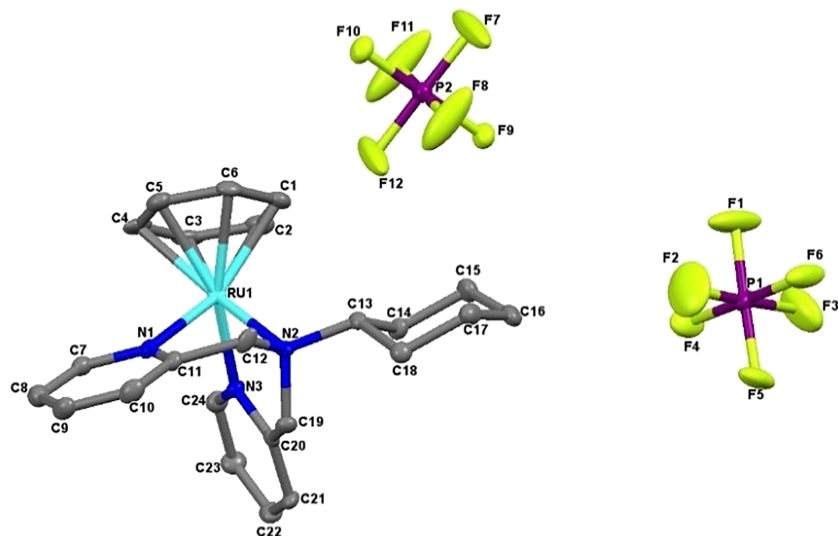


FIGURE 4 Single crystal structure of complex **3** drawn at 50% thermal ellipsoid probability, with omission of hydrogen atoms for clarity

TABLE 2 Selected bond lengths (Å) and angles (°) for complexes **1–3**

	1	2	3
N(1)-Ru(1)	2.173(2)	2.242(3)	2.090(5)
N(2)-Ru(1)	2.098(3)	2.082(3)	2.177(4)
N(3)-Ru(1)	2.082(3)	2.089(3)	2.091(5)
N(2)-Ru(1)-N(3)	79.05(10)	78.66(12)	88.66(19)
N(2)-Ru(1)-N(1)	80.63(10)	79.23(12)	76.22(18)
N(3)-Ru(1)-N(1)	79.24(10)	78.66(12)	88.66(19)

coordination sphere to potential binding substituents compared to the geometry of complexes **1** and **2**. The trend observed provides a direct correlation between the steric size of the central N-donor substituents and the bite angles, which relates to the ability of the metal ion to accommodate and coordinate substrates during catalytic transformations.^[46–48] Furthermore, the dissection angle defined by the planes of the [N(1), C(7), C(8), C(9), C(10), C(11)] and [N(3), C(20), C(21), C(22), C(23), C(24)] pyridyl rings is seen to be acute at 88.31°. This deviates significantly to the equivalent angles of complexes **1** and **2**, with angles of 63.13° and 63.34°, respectively. This effect is rationalized through twisting of the methylene linker on the side of the [N(3), C(20), C(21), C(22), C(23) and C(24)] pyridyl ring.

In complex **4**, the arrangement of the chlorine atom is oriented on the same side as the phenyl moiety due to the reduced steric bulk of this complex.¹⁵ The intersecting angle between the planes of the phenyl group [C(7), C(8), C(9), C(10), C(11) and C(12)] and the Ru(1)-N(1)-C(13)-C(14)-N(2) metallacycle of 45.91° is similar to those reported for related compounds.¹⁵ In this complex, the benzene ring is bound most weakly to the Ru centre with a Ru-Cg distance of 1.664 Å. Apart from a reduced flow of electrons from the benzene moiety to the Ru, evidenced by their increased distance from each other, a further reduction in electron density at the Ru metal is observed due to lengthening of the N(1)-Ru(1) bond (2.159 (2) Å) as shown in Table 3.

TABLE 3 Selected bond lengths (Å) and angles (°) for complex **4**

	4
N(1)-Ru(1)	2.159(2)
N(2)-Ru(1)	2.082(2)
Cl(1)-Ru1	2.3839(7)
N1-Ru(1)-Cl(1)	82.11(7)
N2-Ru(1)-Cl(1)	86.07(6)
N2-Ru(1)-N(1)	76.06(9)

The crystal structure of **1** shows non-covalent interactions of C-H...F bonds (supplementary information, Figure S1). The PF₆[−] counter ion is involved in C-H...F non-covalent intermolecular interactions. Non-classical intermolecular interactions are observed between two F atoms on the PF₆[−] counterion and two H atoms on the pyridine ring. The H...F distances in these interactions are 2.382 and 2.519 Å, respectively with C-H...F angles of 151.69° and 131.43°, respectively. The second interaction exists between two benzene hydrogen bonds and the PF₆[−] (F) atom with H...F distances of 2.584 and 2.487 Å, respectively and C-H...F angles of 120.38° and 124.43°, respectively (Figure S1).

3.2 | Oxidation of *n*-octane catalyzed by **1–4**

All Ru complexes were tested in the C-H bond activation of *n*-octane using two oxidants, *t*-BuOOH (70% in H₂O) and H₂O₂ (30% in H₂O). Reactions were tracked by GC and PPh₃ was added (to reduce any hydroperoxides) when reactions were stopped at either 12 or 27 hr when reactions were deemed complete. Results reported are after PPh₃ addition and from a series of experiments investigating product yields, the optimum octane to oxidant ratio using *t*-BuOOH (~32 mmol) and H₂O₂ (~42 mmol) was established at 1:12. The optimum temperature for all reactions employing both oxidants was 80 °C, with the highest oxygenate selectivity occurring by 12 and 27 hr for the Ru/*t*-BuOOH and Ru/H₂O₂ systems, respectively. Under the established optimum conditions, blank reactions with no added complex were carried out, where a yield of 5% was seen using *t*-BuOOH, whilst a 4% yield was noted for reactions employing H₂O₂. Furthermore, blank reactions with the Ru precursor gave yields of 13% and 6% for the *t*-BuOOH and H₂O₂ systems, respectively (Table 4). In the Ru/*t*-BuOOH reactions, product yields were slightly lower compared to the results when the Ru salt was used as catalyst and may be attributed to the ligand induced steric effects around the metal. Confirmation of the stability of cyclopentanone with *t*-BuOOH and H₂O₂ is shown in the supplementary material (Figure S2).

Results of the catalytic study employing compounds **1–3** with *t*-BuOOH show that compound **2** (entry 4) gives a yield of 12% to C8 oxygenates after 12 hr, whilst **3** (entry 7) was the least active, with a yield of 7% (Table 4). All compounds (**1–3**) were more selective to alcohols over 12 hr (Figure 6A). The benzene ring can dissociate from the metal (as for example shown by the NMR spectrum of the recovered catalyst **1** from the reaction of complex **1**, designated **1R**, Figure 7). Thus, compounds **1–4** are

TABLE 4 Optimum conditions and catalytic testing of *n*-octane over 1–4

Entry	Complex	Oxidant	Substrate: Oxidant	Complex loading (mol%) ^a	Product yield (mol%) ^b	TON ^c
1	-	<i>t</i> -BuOOH	1:12	-	5	-
2	Ru salt	<i>t</i> -BuOOH	1:12	1	13	13
3	1	<i>t</i> -BuOOH	1:12	1	8	8
4	2	<i>t</i> -BuOOH	1:12	1	12	12
5	2	<i>t</i> -BuOOH	1:12	0.01	9	900
6	2	<i>t</i> -BuOOH	1:12	0.1	9	90
7	3	<i>t</i> -BuOOH	1:12	1	7	7
8	4	<i>t</i> -BuOOH	1:12	1	12	12
9	-	H ₂ O ₂	1:12	-	4	-
10	Ru salt	H ₂ O ₂	1:12	1	6	6
11	1	H ₂ O ₂	1:12	1	23	23
12	2	H ₂ O ₂	1:12	1	27	27
13	3	H ₂ O ₂	1:12	1	32	32
14	3	H ₂ O ₂	1:12	0.01	24	2400
15	3	H ₂ O ₂	1:12	0.1	33	330
16	4	H ₂ O ₂	1:12	1	7	7

^a1 mol compound: 100 mol octane (1 mol%), 1 mol compound: 1000 mol octane (0.1 mol%), 1 mol compound: 10 000 mol octane (0.01 mol%) using cyclopentanone (~10 mg) as the internal standard and reactions times of 12 and 27 hours for *t*-BuOOH (32 mmol) and H₂O₂ (42 mmol), respectively.

^bTotal moles of product/initial moles octane.

^cTON = moles total products (mol)/moles of compound (mol).

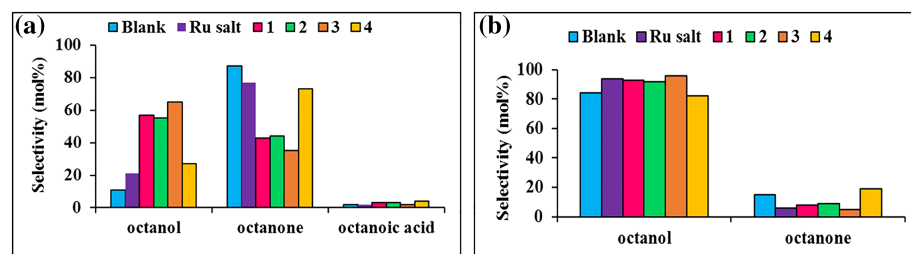


FIGURE 6 A Product distribution profile for compounds 1–4 with *t*-BuOOH over 12 h at 80 °C B Product distribution profile for compounds 1–4 with H₂O₂ over 27 hr at 80 °C

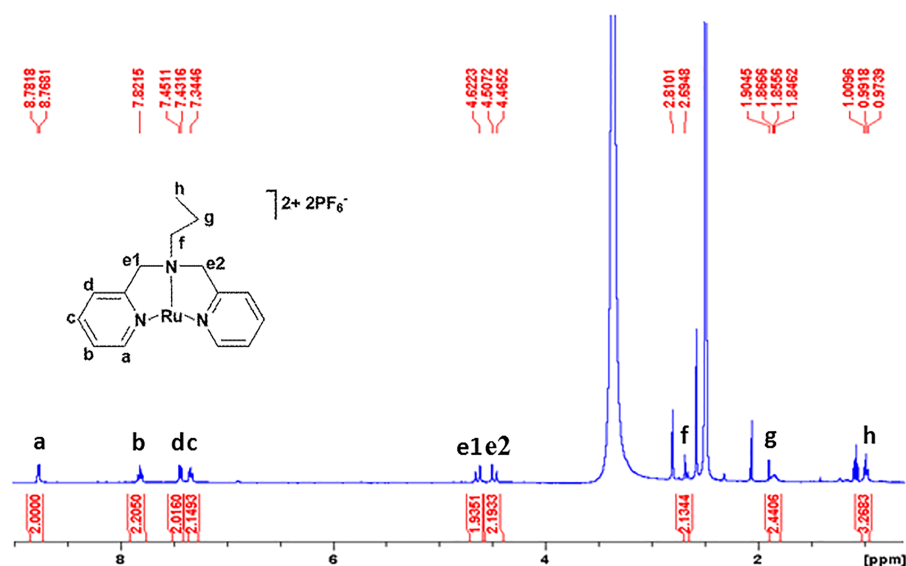


FIGURE 7 NMR spectrum of the compound recovered after the reaction of catalyst 1, (1R)

really 18 electron pre-catalysts, that lose benzene to give the active catalytic species. This allows for easier binding of the substrate to the metal center, which supports the observed degree of over-oxidation (Figure 6A). In the case of **1**, the free rotation of the propyl group may allow for improved accommodation of the substrate and consequently higher yields, which in turn offers less control over the primary product selectivity, and hence a higher production of ketones. The production of ketones was also dominant in the blank reaction (no added complex) as well as the experiment with the Ru salt as catalyst further highlighting the ligand effect. The product distribution profile for **2** is presented in the supporting information (Figure S3).

The activation of the terminal hydrocarbon, C(1), tends to be very difficult as 2° carbons are substantially more reactive than 1° carbons. However, compounds **1–3** produce 1-octanol and octanoic acid over 12 hr with *t*-BuOOH as oxidant (Table 4). It has been well documented that catalytic intermediates can be selective when controlled by free energies of activation and therefore C-H bond cleavage at the terminal carbon can be achieved if the system is sufficiently reactive to cleave a strong bond.^[15,43,49]

With H₂O₂ as oxidant, **3** was most active with a total product yield of 32% (entry 13, Table 4) at the end of 27 hr. Monitoring the reactions over time showed that the C8 oxygenate production rate decreased until 27 hr when the formation effectively stopped. *n*-Octane conversion does continue, however, high boiling side products form, such as dioctyl ether, from secondary reactions. The product distribution profile for **3** over 27 h is given in the supplementary information (Figure S4).

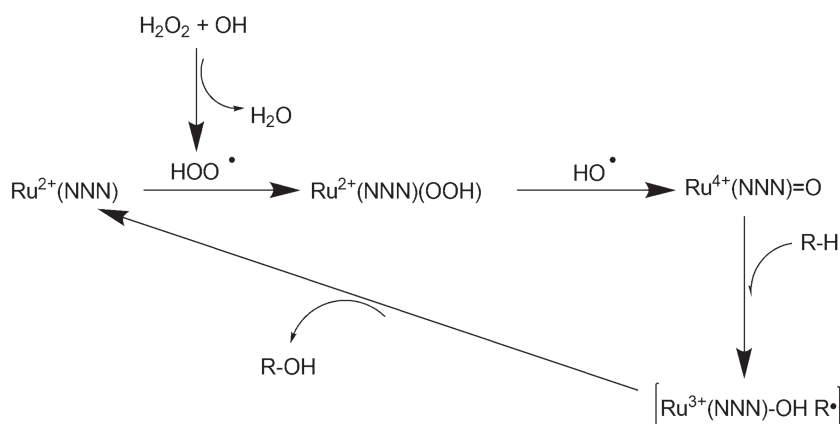
It is seen that complexes **1–3**, with H₂O₂, behave differently than with *t*-BuOOH. The efficiency of each system was influenced by ligand rigidity, as well as electronic factors, and all systems with H₂O₂ are active over longer reaction times compared to those with *t*-BuOOH. The complexes with H₂O₂ showed better results

than with *t*-BuOOH. The product distribution profiles show high formation of alcohols, once alkylhydroperoxides formed in solution were reduced by PPh₃, over 27 hr (including reactions with no added compound and Ru salt) with very low selectivity to ketones (Figure 6B), which may be due to a slower reaction rate than with *t*-BuOOH. The GC profile of the product mixture after workup is shown in Figure S5. Previous reports have shown a promoting effect of water in the catalysis with H₂O₂.^[50–52] Furthermore, the water in H₂O₂ solutions has been suggested to be directly involved in generating hydroxyl radicals.^[53,54] This, however, does not apply to the *t*-BuOOH systems, where an experiment done to investigate this, using **3**, added water and *t*-BuOOH as oxidant, shows a lower yield of 6% (8% yield prior to dilution with water) after 15 hours. Overall, the high yield of oxygenates over complexes **1–3** may be associated to the pincer complexes being largely responsible for stabilizing the Ru-OH intermediate in Scheme 2, prior to the production of alcohols, and/or promote the formation of OH radicals.

Using **2**, 2-octanol as a substrate and *t*-BuOOH as the oxidant, gave a 100% yield to the corresponding ketone within 3 hours, whilst oxidation by H₂O₂ over **3**, showed a yield of only 2% after 3 hr. It is thus noted that with the *t*-BuOOH systems, over-oxidation is fairly rapid over the complexes (all of the 2-octanol is oxidized to the ketone rapidly), however, in the H₂O₂ systems, over-oxidation is slow in the presence of the complex.

The reaction of 1-octanol as substrate with H₂O₂ gave 1% yield to octanal in the presence of **3** over 9 hours. Thus, it is seen that deeper oxidation at the terminal carbon is very slow (in the presence and absence of complex with H₂O₂), since the blank reactions (no complex) of the alcohol also showed yields of only 1% in 9 hr. It thus seems that the Ru compound with H₂O₂ causes very little or no deeper oxidation.

The TON data for the oxidation of *n*-octane in Table 4 with *t*-BuOOH, shows **2** with a TON of 12, whilst **1** and **3**



SCHEME 2 Proposed mechanism for the oxidation of *n*-octane catalysed by **1–4** with H₂O₂

were the least active with TONs of 8 and 7, respectively. Looking at the TONs with H₂O₂, it is seen that compounds **1–3** are between two and four times more efficient in the presence of this oxidant when compared to *t*-BuOOH. The most efficient system was **3** with a TON of 32. Again, these results show that H₂O₂ is a better oxidant than *t*-BuOOH, in that the complexes are more active and efficient over longer reaction periods. Reducing the complex loading to 0.1 mol% and 0.01 mol% of **2** and **3**, respectively, show that a complex loading of 0.01 mol% with *t*-BuOOH gives a TON of 900. With H₂O₂, a compound loading of 0.01 mol% gave a TON of 2400.

Table 5 illustrates the regioselective parameter C(1):C(2):C(3):C(4) over all Ru complexes, which provides information on the reactivity of the hydrogens at carbon positions 1, 2, 3 and 4 of the hydrocarbon chain. These are normalized by accounting for the number of hydrogens present on each carbon atom.^[55] Compound **3** was most selective to the alcohol products at all positions (entries 3 and 7) due to the bulkiness of the ligand compared to compounds **1** and **2** (entries 1, 2, 5 and 6). It was observed that C(2) was the dominant position of attack, as this carbon position is more susceptible to oxidation compared to C(1), and according to thermodynamic calculations (ΔG) this gives the most stable product.^[56] Complexes (**1–3**) were also highly selective to alcohol products after workup at all carbon positions within 27 hr of reaction employing H₂O₂ in the system (Table 5 and Figure S6). Consequently, the selectivity towards the formation of ketones was very low. In a study by Pompeiro *et al.*, homogeneous and immobilized Mn (salen) complexes employing *t*-BuOOH as oxidant were investigated. The authors noted no activation at the primary carbon position and low regioselectivity profiles to the

internal carbon positions of the *n*-octane chain was observed with reported ratios of 1:1:1.3 and 1.7:1:1.1.^[57] Furthermore, the reported selectivity parameters in the *n*-octane activation by *t*-BuOOH was different to literature values involving OH• but was comparable to those involving the generation of *t*BuO•. In another report by Shul'pin and co-workers investigating the oxidation of *n*-octane over NaVO₃, high regioselective ratios of 1:10.1:10.7:8.4 and 1:7:6:5 were obtained in MeCN and H₂O, respectively employing H₂O₂ and H₂SO₄ as co-catalysts.^[58] With the observed selectivity parameters, the octane oxidation reaction was thought to proceed *via* the formation of OH•. Another study investigating the oxidation by *t*-BuOOH of *n*-octane over SNS ligand catalysts with varying N-donor backbones (pyridine and amine) revealed a high selectivity to octanones over the amine-based SNS catalyst with regioselective ratios of 1.4:1.1:1 to the C(2), C(3) and C(4) positions. In contrast, pyridine-based complexes were more selective to the octanol, specifically, 1-octanol and 2-octanol, giving a total regioselectivity ratio of 1:5.6:3.9:4.2. The authors suggested that the rigid pyridine backbone of the SNS complexes hindered over-oxidation compared to the less rigid amine-based SNS compounds.^[59] A different study showed that the C(2) position was the most activated carbon of the *n*-octane chain over Co PNP complexes bearing a pentyl and iso-propyl moiety on the central nitrogen donating atom. These complexes gave regioselectivity parameters of 1:4.2:4.2:2.9 and 1:4.2:2.9:2.9, respectively with some activation at the C(1) position.^[55]

With the bidentate compound **4**, the catalytic study with *t*-BuOOH (entry 8, Table 4) shows a yield of 12% to C8 products after 12 hr. The high catalytic activity shown

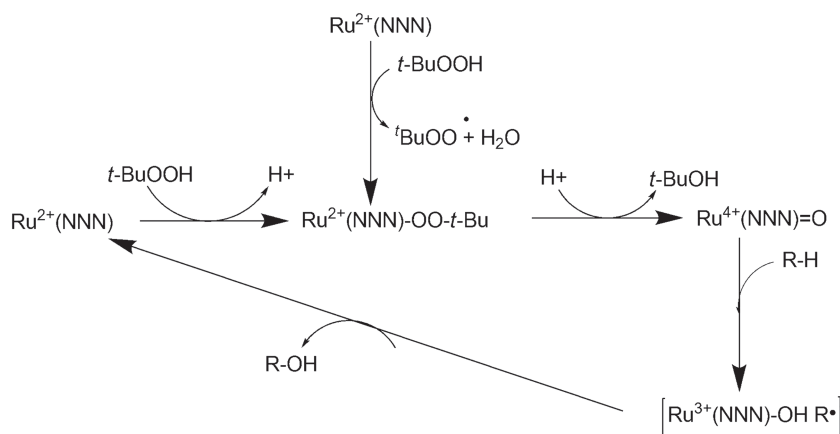
TABLE 5 Regioselectivity parameters C(1):C(2):C(3):C(4) in the oxidation of *n*-octane by *t*-BuOOH and H₂O₂ over **1–4**

Entry	Complex	Oxidant	Alcohol	Ketone	Total ^a	A/K ^b
			C(1):C(2):C(3):C(4)	C(2):C(3):C(4)	C(1):C(2):C(3):C(4)	
1	1	<i>t</i> -BuOOH	1:13.5:6.5:7	1.8:2:1	1:7.7:4.3:4	
2	2	<i>t</i> -BuOOH	0.3:13.5:6.5:7	2.1:1.9:1	1:17.3:11.5:8.8	1.2:1
3	3	<i>t</i> -BuOOH	1:21.4:10.7:12.9	1.8:1.6:1	1:21.8:13.2:13	2:1
4	4	<i>t</i> -BuOOH	0:1.9:1:1	2:1.8:1	0:2:1.4:1	0.4:1
5	1	H ₂ O ₂	1:5:4:5	1.5:1.5:1	1:6.5:5.5:6	13:1
6	2	H ₂ O ₂	1:5.6:4.4:5.6	1.5:2:1	1:7.1:6.4:6.6	12:1
7	3	H ₂ O ₂	1:5.2:4.2:5.2	2:2:1	1:7.2:6.2:6.2	24:1
8	4	H ₂ O ₂	1:5.2:5:6.1	1.8:2:1	1:7:7:7.1	5:1

^aThe total regioselective parameter accounts for all products (octanones, octanols, octanal and octanoic acid). All reactions were carried out at 80 °C with a compound loading of 1 mol% (0.008 mmol), an octane to oxidant ratio of 1:12 for both *t*-BuOOH (32 mmol) and H₂O₂ (42 mmol), cyclopentanone as the internal standard (~10 mg) and reaction times of 12 and 27 hours for *t*-BuOOH and H₂O₂, respectively.

^bAlcohol: Ketone ratio.

SCHEME 1 Proposed mechanism for the oxidation of *n*-octane catalysed by **1–4** with *t*-BuOOH



by **4** is likely due to a less sterically hindered metal center through loss of the benzene ring during the catalysis. From this, a higher catalytic activity might be expected, however, the phenyl substituted N-donor backbone, that is largely electron withdrawing by the resonance effect, also influences the activity. The cleavage of the benzene ring, together with the lower steric effect of the bidentate ligand, allows for enhanced access to the metal center, which relates to the observed elevated production of ketones (Figure 6A).

With H₂O₂, complex **4** was less active, giving a total yield of 7% at the end of 27 hr (entry 16, Table 4). This could be due to a lower concentration of OH• generated, that essentially gives a low yield, when compared to the pincer compounds. In addition, the low yield could be further due to the electronic effect that stems from the presence of the electron withdrawing phenyl moiety on the nitrogen backbone of the compound. Looking at the regioselective parameter C(1):C(2):C(3):C(4) over compound **4**, the lowest selectivity towards alcohols was observed (entry 4, Table 5) with *t*-BuOOH. Again, C(2) was the dominant position of attack, producing the most stable products.

Adding the radical scavenger TEMPO to the reaction mixture resulted in a drop in yield from 12% to 4% over the [Ru{pyCH₂NC(CH₃)₃CH₂py}C₆H₆]/*t*-BuOOH system, whilst no product yield was observed over 27 hours for the [Ru{pyCH₂NC₆H₁₁CH₂py}C₆H₆]/H₂O₂ compound, implying that a radical initiated mechanism is followed when using both oxidants. Since alcohols are formed dominantly by reaction of these compounds with *n*-octane involving both oxidants (except for **4** with *t*-BuOOH), consistent with the analytical method employed, two kinds of mechanisms can be proposed for the oxidation with H₂O₂ or *t*-BuOOH catalyzed by Ru (Schemes 1 and 2).

In Scheme 1, the Ru²⁺(NNN) complex reacts with *t*-BuOOH to produce an alkylperoxy-ruthenium (II)

complex. This complex then provides an oxo-ruthenium (IV) species, through homolytic cleavage of the O-O bond in the alkylperoxy-ruthenium (II) complex. Abstraction of a hydrogen atom from the hydrocarbon *via* the oxo-ruthenium (IV) species gives a Ru³⁺OHR• radical. The catalytic cycle becomes complete upon transfer of the hydroxy ligand to the R• radical which affords the alcohol, ROH and the Ru²⁺(NNN) species.^[60] Further oxidation of the secondary alcohols results in the corresponding ketones as observed over **4** with *t*-BuOOH. In H₂O₂, a similar mechanism is proposed as outlined for *t*-BuOOH (Scheme 1), but instead proceeds *via* an OH radical to give the oxo-ruthenium (IV) species (Scheme 2).

4 | CONCLUSION

A set of Ru pyridine-based compounds with aliphatic and aromatic N-donor backbones was synthesized. Single crystal XRD further confirmed the formation of pincer complexes in the case of **1–3** and a bidentate complex for **4**. The catalytic testing of complexes **1–4** using two oxidants, *tert*-butylhydroperoxide and hydrogen peroxide, and *n*-octane as a substrate, showed that with *t*-BuOOH, the most active compounds were **2** and **4** with a yield of 12%. All complexes (except for **4** with *t*-BuOOH) gave high selectivities to alcohols utilizing both oxidants. Employing H₂O₂ in the catalysis showed considerably improved activity for the pincer compounds in the oxidation of *n*-octane with H₂O₂ forming more alcohols compared to *t*-BuOOH, which may be due to stabilization of the intermediate, Ru³⁺(NNN)-OH R•, or be responsible for promoting OH• formation. Compound **3** showed the highest activity, giving a 32% yield. 2-Octanol was the dominant product observed over the Ru/*t*-BuOOH and Ru/H₂O₂ systems. Furthermore, 1-octanol was also produced over the [Ru{pyCH₂NC₆H₁₁CH₂py}C₆H₆]/

t-BuOOH and [Ru{pyCH₂N(R)py}C₆H₆]/H₂O₂ systems. Time-dependent studies reveal that over-oxidation is more prominent with *t*-BuOOH than with H₂O₂. Very good TONs were achieved with both oxidants, however, H₂O₂ gave higher TONs than *t*-BuOOH.

ACKNOWLEDGMENTS

We are grateful to the University of KwaZulu-Natal, the Department of Science and Technology - National Research Foundation Centre of Excellence in Catalysis, c*change, (PAR 06.2) and the National Research Foundation (Grant no. 111508) for financial assistance. The authors gratefully acknowledge Dr Michael Nivendran Pillay and Mr Sizwe Zamisa for x-ray crystallographic data collection and refinement, and Dr. S. Alapour for a valuable discussion.

ORCID

Holger B. Friedrich  <https://orcid.org/0000-0002-1329-0815>

Mzamo L. Shozi  <https://orcid.org/0000-0001-7666-2543>

REFERENCES

- [1] V. R. Landaeta, R. E. Rodríguez-Lugo, *J. Mol. Catal. A: Chem.* **2017**, *426*, 316.
- [2] K. Liao, S. Negretti, D. G. Musaev, J. Bacsá, H. M. Davies, *Nature* **2016**, *533*, 230.
- [3] M. S. Chen, M. C. White, *Science* **2010**, *327*, 566.
- [4] X. Tang, X. Jia, Z. Huang, *Chem. Sci.* **2018**, *9*, 288.
- [5] M. T. Whited, R. H. Grubbs, *Acc. Chem. Res.* **2009**, *42*, 1607.
- [6] J. T. Singleton, *Tetrahedron* **2003**, *59*, 1837.
- [7] W. Baratta, G. Chelucci, E. Herdtweck, S. Magnolia, K. Siega, P. Rigo, *Angew. Chem. Int. Ed.* **2007**, *46*, 7651.
- [8] F. Hana, A. J. Lough, G. G. Lavoie, *Dalton Trans.* **2017**, *46*, 16228.
- [9] Z. Chval, O. Dvořáčková, D. Chvalová, J. V. Burda, *Inorg. Chem.* **2019**, *58*, 3616.
- [10] F. Zeng, Z. Yu, *Organometallics* **2008**, *27*, 2898.
- [11] C. Gunanathan, D. Milstein, *Chem. Rev.* **2014**, *114*, 12024.
- [12] F. Zeng, Z. Yu, *Organometallics* **2009**, *28*, 1855.
- [13] S. K. Sarkar, M. S. Jana, T. K. Mondal, C. Sinha, *Appl. Organomet. Chem.* **2014**, *28*, 641.
- [14] E. A. Nyawade, H. B. Friedrich, B. Omondi, P. Mpungose, *Organometallics* **2015**, *34*, 4922.
- [15] J. M. Gichumbi, H. B. Friedrich, B. Omondi, *Transit. Metal Chem.* **2016**, *41*, 867.
- [16] T. Kojima, T. Sakamoto, Y. Matsuda, *Inorg. Chem.* **2004**, *43*, 2243.
- [17] J. H. Wallenstein, J. Sundberg, C. J. McKenzie, M. Abrahamsson, *Eur. J. Inorg. Chem.* **2016**, *2016*, 897.
- [18] J. Bjernemose, A. Hazell, C. J. McKenzie, M. F. Mahon, L. P. Nielsen, P. R. Raithby, O. Simonsen, H. Toflund, J. A. Wolny, *Polyhedron* **2003**, *22*, 875.
- [19] F. Weisser, S. Plebst, S. Hohloch, M. van der Meer, S. Manck, F. Führer, V. Radtke, D. Leichnitz, B. Sarkar, *Inorg. Chem.* **2015**, *54*, 4621.
- [20] Z. Shirin, R. Mukherjee, J. F. Richardson, R. M. Buchanan, *J. Chem. Soc. Dalton Trans.* **1994**, 465.
- [21] T. Kojima, T. Morimoto, T. Sakamoto, S. Miyazaki, S. Fukuzumi, *Chem. – Eur. J.* **2008**, *14*, 8904.
- [22] A. Li, J. K. White, K. Arora, M. K. Herroon, P. D. Martin, H. B. Schlegel, I. Podgorski, C. Turro, J. J. Kodanko, *Inorg. Chem.* **2016**, *55*, 10.
- [23] R. Chanerika, H. B. Friedrich, M. L. Shozi, *Inorg. Chim. Acta.* <https://doi.org/10.1016/j.ica.2019.118992>
- [24] M. A. Bennett, A. K. Smith, *J. Chem. Soc. Dalton Trans.* **1974**, 233.
- [25] Bruker, *APEXII*, Bruker AXS Inc., Madison, Wisconsin, USA **2009**.
- [26] Bruker, *SAINTE, XPREP and SADABS*, Bruker AXS Inc., Madison, WI, USA **2009**.
- [27] Bruker, *SADABS*, Bruker AXS Inc., Madison, WI, USA **2009**.
- [28] Bruker, *SHELXL, XS, XL, XP, XSELL*, Bruker AXS Inc., Madison, WI, USA **2009**.
- [29] A. L. Spek, *J. Inorg. Crystallogr.* **2003**, *36*, 7.
- [30] L. J. Barbour, *Supramol. Chem.* **2001**, *1*, 189.
- [31] J. L. Atwood, L. J. Barbour, *Cryst. Growth des.* **2003**, *3*, 3.
- [32] POVray. Persistence of Vision Raytracer 3.6.
- [33] C. F. Macrae, I. J. Bruno, J. A. Chisholm, P. R. Edgington, P. McCabe, E. Pidcock, L. Rodriguez-Monge, R. Taylor, J. van de Streek, P. A. Wood, *J. Appl. Crystallogr.* **2008**, *41*, 466.
- [34] D. Gonzalez Cabrera, B. D. Koivisto, D. A. Leigh, *Chem. Commun.* **2007**, 4218.
- [35] K. Visvaganesan, R. Mayilmurugan, E. Suresh, M. Palaniandavar, *Inorg. Chem.* **2007**, *46*, 10294.
- [36] H. Mishra, A. K. Patra, R. Mukherjee, *Inorg. Chim. Acta* **2009**, *362*, 483.
- [37] E. R. Milaeva, D. B. Shpakovsky, Y. A. Gracheva, S. I. Orlova, V. V. Maduar, B. N. Tarasevich, N. N. Meleshonkova, L. G. Dubova, E. F. Shevtsova, *Dalton Trans.* **2013**, *42*, 6817.
- [38] D. Gallego, S. Inoue, B. Blom, M. Driess, *Organometallics* **2014**, *33*, 6885.
- [39] D. Kim, S. Kim, E. Kim, H. J. Lee, H. Lee, *Polyhedron* **2013**, *63*, 139.
- [40] Q. Major, A. J. Lough, D. G. Gusev, *Organometallics* **2005**, *24*, 2492.
- [41] G. M. Adams, A. S. Weller, *Coord. Chem. Rev.* **2018**, *355*, 150.
- [42] P. Pattanayak, D. Patra, P. Brandão, D. Mal, V. Felix, *Inorg. Chem. Commun.* **2015**, *53*, 68.
- [43] C. Xu, X. C. Liu, X. D. Jin, Q. Yang, G. C. Han, Y. C. Gang, H. H. Hu, *J. Coord. Chem.* **2014**, *67*, 352.
- [44] M. Uršič, T. Lipeč, A. Meden, I. Turel, *Molecules* **2017**, *22*, 326.
- [45] J. M. Gichumbi, H. B. Friedrich, B. Omondi, *J. Mol. Catal. A: Chem.* **2016**, *416*, 29.
- [46] S.-Q. Bai, L. L. Koh, T. S. A. Hor, *Inorg. Chem.* **2009**, *48*, 1207.
- [47] M. Blumenkemper, H. Schröder, T. Pape, F. E. Hahn, *Inorg. Chim. Acta* **2012**, *390*, 143.
- [48] R. J. Ball, A. R. J. Genge, A. L. Radford, B. W. Skelton, V.-A. Tolhurst, A. H. White, *J. Chem. Soc. Dalton Trans.* **2001**, 2807.
- [49] J. F. Hartwig, M. A. Larsen, *ACS Cent. Sci.* **2016**, *2*, 281.
- [50] T. A. Fernandes, V. André, A. M. Kirillov, M. V. Kirillova, *J. Mol. Catal. A: Chem.* **2017**, *426*, 357.
- [51] T. A. Fernandes, C. I. M. Santos, V. André, J. Klak, M. V. Kirillova, A. M. Kirillov, *Inorg. Chem.* **2016**, *55*, 125.

- [52] T. A. Fernandes, C. I. M. Santos, V. Andre, S. S. P. Dias, M. V. Kirillova, A. M. Kirillov, *Catal. Sci. Technol.* **2016**, *6*, 4584.
- [53] M. V. Kirillova, M. L. Kuznetsov, V. B. Romakh, L. S. Shul'pina, J. J. R. Fraústo da Silva, A. J. L. Pombeiro, G. B. Shul'pin, *J. Catal.* **2009**, *267*, 140.
- [54] M. L. Kuznetsov, A. J. L. Pombeiro, *Inorg. Chem.* **2009**, *48*, 307.
- [55] D. Naicker, H. B. Friedrich, B. Omondi, *RSC Adv.* **2015**, *5*, 63123.
- [56] V. D. B. C. Dasireddy, H. B. Friedrich, S. Singh, *Appl. Catal., A* **2013**, *467*, 142.
- [57] T. C. O. Mac Leod, M. V. Kirillova, A. J. L. Pombeiro, M. A. Schiavon, M. D. Assis, *Appl. Catal., A* **2010**, *372*, 191.
- [58] L. S. Shul'pina, M. V. Kirillova, A. J. L. Pombeiro, G. B. Shul'pin, *Tetrahedron* **2009**, *65*, 2424.
- [59] L. Soobramoney, M. D. Bala, H. B. Friedrich, *Dalton Trans.* **2014**, *43*, 15968.
- [60] S. I. Murahashi, N. Komiya, Y. Oda, T. Kuwabara, T. Naota, *J. Org. Chem.* **2000**, *65*, 9186.

SUPPORTING INFORMATION

Additional supporting information may be found online in the Supporting Information section at the end of this article.

How to cite this article: Chanerika R, Friedrich HB, Shoji ML. Application of new Ru (II) pyridine-based complexes in the partial oxidation of *n*-octane. *Appl Organometal Chem.* 2019;e5361. <https://doi.org/10.1002/aoc.5361>